

SPREADING OF ACCRETED MATERIAL ON WHITE DWARFS

ANTHONY L. PIRO

Department of Physics, Broida Hall, University of California
Santa Barbara, CA 93106; piro@physics.ucsb.edu

AND

LARS BILDSTEN

Kavli Institute for Theoretical Physics and Department of Physics, Kohn Hall, University of California
Santa Barbara, CA 93106; bildsten@kitp.ucsb.edu

Draft version November 6, 2018

ABSTRACT

When a white dwarf (WD) is weakly magnetized and its accretion disk is thin, accreted material first reaches the WD's surface at its equator. This matter slows its orbit as it comes into co-rotation with the WD, dissipating kinetic energy into thermal energy and creating a hot band of freshly accreted material around the equator. Radiating in the extreme ultraviolet and soft X-rays, this material moves toward the pole as new material piles behind it, eventually becoming part of the WD once it has a temperature and rotational velocity comparable with the surface. We present a set of solutions which describe the properties of this “spreading layer” in the steady state limit based on the conservation equations derived by Inogamov & Sunyaev (1999) for accreting neutron stars. Our analysis and subsequent solutions show that the case of WDs is qualitatively different. We investigate example solutions of the spreading layer for a WD of mass $M = 0.6M_{\odot}$ and radius $R = 9 \times 10^8$ cm. These solutions show that the spreading layer typically extends to an angle of $\theta_{\text{SL}} \approx 0.01 - 0.1$ (with respect to the equator), depending on accretion rate and the magnitude of the viscosity. At low accretion rates, $\dot{M} \lesssim 10^{18}$ g s⁻¹, the amount of spreading is negligible and most of the dissipated energy is radiated back into the accretion disk. When the accretion rate is high, such as in dwarf novae, the material may spread to latitudes high enough to be visible above the accretion disk. The effective temperature of the spreading layer is $\sim (2-5) \times 10^5$ K with approximately $T_{\text{eff}} \propto \dot{M}^{9/80}$. This power-law dependence on \dot{M} is weaker than for a fixed radiating area and may help explain extreme ultraviolet observations during dwarf novae. We speculate about other high accretion rate systems ($\dot{M} \gtrsim 10^{18}$ g s⁻¹) which may show evidence for a spreading layer, including symbiotic binaries and supersoft sources.

Subject headings: accretion, accretion disks — novae, cataclysmic variables — stars: dwarf novae — white dwarf — X-rays: stars

1. INTRODUCTION

In close binaries containing a white dwarf (WD), the companion star can fill its Roche lobe either through stellar evolution or angular momentum loss and begin accreting onto the WD to form a cataclysmic variable (CV; Warner 1995). Before material can reach the WD it must transport angular momentum outward via an accretion disk. Observations and theoretical studies show that when the disk can radiate the internally dissipated energy (Pringle 1981) it will be thin (i.e. the vertical height of the disk is much smaller than the WD radius; Shakura & Sunyaev 1973; Meyer & Meyer-Hofmeister 1982) and rotating at nearly Keplerian velocity. If the WD is weakly magnetized, the accreted material reaches the surface at the equator and then must pass through a transition region to settle into the WD and become part of the star. When the WD spin is much less breakup, nearly half of the accretion luminosity is released in this region, making it as luminous as the accretion disk and likely crucial to understanding the luminosity from accreting WDs.

The transition from the accretion disk to the WD surface is typically treated in a boundary layer (BL) model, which is simply an extension of the accretion disk with additional torques provided by the WD to decelerate disk material to the WD rotational velocity. In BL studies the important coordinate is assumed to be radial and the vertical structure is solved by assuming a vertical pressure scale height (e.g. Popham

& Narayan 1995). The geometry of the BL is of a fattened disk near the WD surface. Other BL studies solve the two-dimensional problem simultaneously in both radial and latitudinal directions using numerical techniques (e.g. Kley & Hensler 1987; Kley 1989a, 1989b). Kippenhahn & Thomas (1978) investigated the properties of “accretion belts” on WDs by assuming that the accreted material is marginally stable to the Richardson criterion. We now want to understand the state of recently accreted material on much shorter timescales ($\ll 10^4$ yr), and assess the effects of a turbulent viscous stress on the spreading properties. In Inogamov & Sunyaev (1999; hereafter IS99), this problem was approached from a new angle to study accreting neutron stars (NSs). Their method follows the latitudinal flow of matter on the compact object which provides information about the spreading area of hot, freshly accreted material which is not captured in BL models. We now apply these same methods to the case of WDs and call this model the spreading layer (SL), to differentiate it from BL studies. We solve the conservation equations derived by IS99 for fluid confined to the WD surface and find that the steady state limit naturally attracts toward solutions where local viscous dissipation is nearly balanced by local radiative cooling. This is qualitatively different than the results of IS99 who found that the SLs of NSs show a great deal of advection of dissipated energy up to higher latitudes where it is radiated. This is mainly due to their high accretion rates near the Eddington limit.

For a fiducial WD of mass $M = 0.6M_{\odot}$ and radius $R = 9 \times 10^8$ cm, our solutions yield a thin hot band of extent $\theta_{\text{SL}} \approx 0.01 - 0.1$ with an effective temperature of $\sim (2 - 5) \times 10^5$ K over a range of accretion rates from $10^{17} - 10^{19}$ g s $^{-1}$, implying that the SL should contribute to accreting WD spectra in the extreme ultraviolet (EUV) or soft X-rays. We also find the SL's dependence on accretion rate and viscosity. These solutions show that at low accretion rates ($\dot{M} \lesssim 10^{18}$ g s $^{-1}$) the SL does not appear above the accretion disk, so that radiation from the SL may be obscured by the accretion disk or its winds. Only when $\dot{M} \gtrsim 10^{18}$ g s $^{-1}$, such as in dwarf novae, symbiotic binaries, or supersoft sources, will the SL reach high enough latitudes to be directly seen. Perhaps the best chance for testing the SL model are dwarf novae in outburst and superoutburst. Some observations show a fairly constant effective temperature over a large change in luminosity (for example SS Cyg; Mauche, Raymond & Mattei 1995) which is consistent with a SL. Direct comparisons between our simple model and observations can be complicated if the SL emission is absorbed and re-radiated by accretion disk winds, as is likely for systems which show that the EUV is not eclipsed by the secondary whereas the WD is (such as for the edge-on OY Car in superoutburst; Mauche & Raymond 2000). Nevertheless, the SL may be important for calculating the underlying continuum scattered by these winds. We predict a quick timescale for spreading, $t_{\text{SL}} \sim 50$ s, which means that the typical mass of the spreading region ($\lesssim 10^{20}$ g) is much less than the “accretion belt” of Kippenhahn & Thomas (1978). Most likely, as angular momentum is transferred between the SL and the underlying WD surface, the underlying surface layers will spin up similar to what Kippenhahn & Thomas (1978) calculate. The short spreading timescale also means that following a dwarf nova outburst, when accretion onto the WD has decreased dramatically, the SL will spread over the WD surface too quickly to be observed as a separate hot component.

In §2 we solve for the radial structure of the SL using a one-zone model. We derive the differential equations which describe the SL in the steady state limit in §3, using IS99 as a guide. In §4 we discuss the solutions of the spreading equations. We study physically motivated analytic estimates which capture the essential features of the numerical integrations. These provide power law relations which show how the SL changes with accretion rate, viscosity, and the properties of the accreting WD. We then present the results of integrating the equations numerically to understand the SL in more detail. In §5 we discuss observational tests for the SL and consider the current data in relation to our calculations. We conclude in §6 with a summary of our findings along with a discussion about further work which can be done with this model.

2. RADIAL PROPERTIES OF THE HOT SPREADING LAYER

Following IS99, we first construct a one-zone model to capture the radial extent of the hot, rapidly rotating material in the SL, derived in a frame on the surface of a WD. The SL is assumed to start near the equator in hydrostatic balance. The pressure scale height, $h = P/\rho g \sim 10^7$ cm (this will be shown in §4), is significantly less than the radius of a typical WD so we assume a plane parallel geometry with constant gravitational acceleration. Initially the azimuthal velocity of the spreading material, v_{ϕ} , will be nearly Keplerian, $v_{\phi} \approx v_{\text{K}} \equiv (GM/R)^{1/2}$, so that gravitational acceleration can be significantly decreased by centrifugal effects. We therefore

use an “effective” gravitational constant

$$g_{\text{eff}} = \frac{GM}{R^2} - \frac{v_{\theta}^2}{R} - \frac{v_{\phi}^2}{R}, \quad (1)$$

where v_{θ} is the latitudinal velocity, θ is measured with respect to the equator, and we assume that the WD is rotating much slower than breakup. Since g_{eff} is independent of radius in the thin limit, hydrostatic balance is integrated to give

$$P = g_{\text{eff}}y, \quad (2)$$

where y is the column depth, defined as $dy \equiv -\rho dz$, and z is the radial coordinate in this plane parallel layer.

Radiation pressure may play an important role in the hot SL so we define the force per unit mass due to radiation flux at the photosphere,

$$g_{\text{rad}} = \frac{\kappa F}{c}, \quad (3)$$

where κ is the opacity, F is the flux, and c is the speed of light. If the one-zone layer becomes optically thin we cannot assume the flux provides this force and these approximations become invalid. With these definitions $g_{\text{eff}} = g_{\text{rad}}$ defines the local Eddington accretion rate. We use an opacity dominated by Thomson scattering ($\kappa = 0.34$ g cm $^{-2}$ for a solar composition with mean molecular weight per electron of $\mu_e \approx 1.2$). Free-free absorption may also be an important mechanism for radiative transport so we check our assumption of an electron scattering dominated opacity once we find the numerical solutions for the SL in §4.

We assume that the flux is constant throughout the layer. Implicit in this assumption is that the majority of the dissipation is at the bottom of the layer where hot, rapidly rotating spreading material comes into contact with the cold, slowly rotating WD. Radiative diffusion results in

$$F = \frac{4acT^3}{3\kappa} \frac{dT}{dy}, \quad (4)$$

where a is the radiation constant.

Pressure is related to density and temperature by the equation of state,

$$P = \frac{\rho kT}{\mu m_p} + \frac{aT^4}{3}, \quad (5)$$

where k is Boltzmann's constant and μ is the mean molecular weight ($\mu = 0.62$ for a solar composition). Equation (4) is integrated and combined with equation (5) to give

$$T = \left(\frac{3\kappa F}{ac} \right)^{1/4} y^{1/4}, \quad (6)$$

and

$$\rho = \frac{\mu m_p}{kT} (g_{\text{eff}} - g_{\text{rad}})y. \quad (7)$$

We use equations (2), (6), and (7) to describe the layer, where y is the column depth at the base of the spreading matter. This material will initially have a much higher entropy than the WD surface when it arrives at the equator. As the material moves toward the WD pole it will radiate and slow its rotational velocity until it becomes part of the WD (Figure 1).

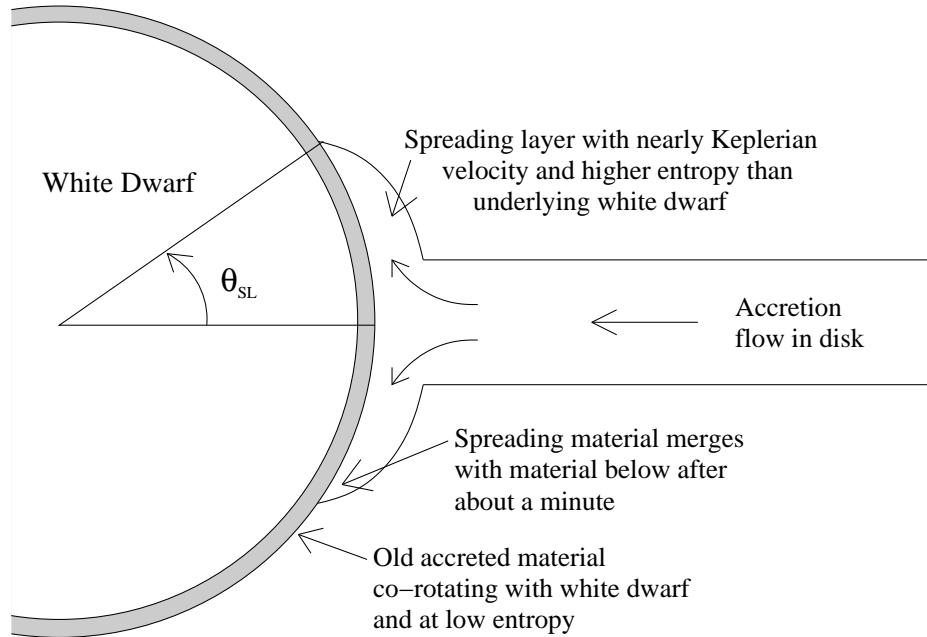


FIG. 1.— A schematic diagram of the spreading layer making contact with the white dwarf. The accretion flow arrives at the white dwarf with nearly Keplerian azimuthal velocity. As material piles at the equator, rotational energy is dissipated, heating the layer. The pressure which is created at the equator forces material toward the pole, creating a spreading layer. The material continues to travel away from the equator until it loses its azimuthal velocity due to frictional dissipation and has an entropy similar to the underlying white dwarf. At this point the spreading material becomes part of the slowly downward advecting material on the white dwarf surface.

3. DERIVATION OF SPREADING EQUATIONS

Since we are primarily interested in how the properties of the accreting material change with latitude, it is easiest to consider the equations for conserved fluxes (fluxing in the θ -direction), integrated radially through the SL. These equations are taken in the steady state limit, resulting in a set of equations analogous to those derived by IS99. We include the majority of the derivation here as it will assist our choice of boundary conditions which is different than what IS99 found for NSs. In our derivation we primarily use notation consistent with IS99, but make changes when convenient to do so.

3.1. Conservation Equations

We first derive the general, time dependent, conservation equations in a frame on the WD. For conservation of mass we consider the radially integrated density (i.e. the column depth, y),

$$\frac{\partial}{\partial t}(2\pi R y \cos \theta) + \frac{1}{R} \frac{\partial}{\partial \theta}(2\pi R y v_{\theta} \cos \theta) = 0, \quad (8)$$

which simplifies to

$$R \cos \theta \frac{\partial y}{\partial t} + \frac{\partial}{\partial \theta}(y v_{\theta} \cos \theta) = 0. \quad (9)$$

Conservation of momentum in the θ -direction is given by

$$\begin{aligned} \frac{\partial}{\partial t}(2\pi R y v_{\theta} \cos \theta) + \frac{1}{R} \frac{\partial}{\partial \theta}(2\pi R y v_{\theta}^2 \cos \theta) + 2\pi R y \frac{v_{\phi}^2}{R} \sin \theta \\ = -2\pi R \cos \theta \frac{1}{R} \frac{\partial}{\partial \theta} \left(\int_0^h P dz \right) - 2\pi R \tau_{\theta} \cos \theta. \end{aligned} \quad (10)$$

which can be rewritten as,

$$\begin{aligned} R \cos \theta \frac{\partial}{\partial t}(y v_{\theta}) + \frac{\partial}{\partial \theta}(y v_{\theta}^2 \cos \theta) + y v_{\phi}^2 \sin \theta \\ = -\cos \theta \frac{\partial}{\partial \theta} \left(\int_0^h P dz \right) - R \tau_{\theta} \cos \theta, \end{aligned} \quad (11)$$

where the last term on the left side is a centrifugal piece which comes from the gradient of the spherical coordinate basis vectors (Landau & Lifshitz 1959), the first term on the right is the radially integrated hydrostatic force, and τ_{θ} is the viscous stress in the θ -direction. The total viscous stress, τ , is from the turbulence created as high entropy fluid quickly rotates against the lower entropy WD material below. We parametrize τ in terms of a unitless constant, α , so that

$$\tau = \alpha \rho v^2, \quad (12)$$

where $v^2 = v_{\theta}^2 + v_{\phi}^2$. In Appendix A we consider lower limits to α provided by ion or radiative viscosities. These are found to be fairly small ($\alpha \lesssim 10^{-6}$), implying that turbulence is probably the dominant cause of friction. To be as general as possible we treat α as a free parameter and study its affect on the spreading properties for the values $\alpha = 10^{-4} - 10^{-2}$. This range of values is chosen for the physically realistic solutions which result for $\dot{M} \sim 10^{17} - 10^{19} \text{ g s}^{-1}$. If $\alpha \lesssim 10^{-4}$ the viscous stress is too slow to halt the spreading, and the spreading flow diverges in numerical integrations. For $\alpha \gtrsim 10^{-2}$ the dissipation becomes so large that the scale height puffs up to be comparable to the WD radius, making the plane parallel assumptions invalid. In such a case a more detailed study of the radial structure is required than what we provide in §2. We discuss the available parameter space for values of α in more detail in §4 when we consider the boundary conditions. The components of τ are

$$\tau_{\theta} = \alpha \rho v^2 \frac{v_{\theta}}{v} = \alpha \rho v_{\theta} \sqrt{v_{\theta}^2 + v_{\phi}^2}, \quad (13)$$

and

$$\tau_{\phi} = \alpha \rho v_{\phi} \sqrt{v_{\theta}^2 + v_{\phi}^2}, \quad (14)$$

in the latitudinal and azimuthal directions, respectively.

The pressure, integrated over a scale height, h , is

$$\begin{aligned} \int_0^h P dz &= \frac{k}{\mu m_p} \left(\frac{3\kappa F}{ac} \right)^{1/4} \frac{g_{\text{eff}}}{g_{\text{eff}} - g_{\text{rad}}} \int_0^y y^{1/4} dy \\ &= \frac{4}{5} \frac{g_{\text{eff}}}{g_{\text{eff}} - g_{\text{rad}}} \frac{kTy}{\mu m_p}, \end{aligned} \quad (15)$$

where both y and T are assumed to be their respective values at the base of the SL, and κ is assumed to be constant. We see that difficulties arise in the one-zone formulation when the SL becomes close to the Eddington limit ($g_{\text{eff}} = g_{\text{rad}}$). This must be carefully considered when we solve the resulting differential equations in §4.

Next, there is conservation of momentum in the ϕ -direction,

$$\begin{aligned} \frac{\partial}{\partial t} (2\pi R y v_\phi \cos \theta) + \frac{1}{R} \frac{\partial}{\partial \theta} (2\pi R y v_\phi v_\theta \cos \theta) \\ - 2\pi R y \frac{v_\theta v_\phi}{R} \sin \theta = -2\pi R \tau_\phi \cos \theta. \end{aligned} \quad (16)$$

Simplifying this expression we find,

$$\begin{aligned} R \cos \theta \frac{\partial}{\partial t} (y v_\phi) + \frac{\partial}{\partial \theta} (y v_\phi v_\theta \cos \theta) - y v_\phi v_\theta \sin \theta \\ = -R \tau_\phi \cos \theta, \end{aligned} \quad (17)$$

where τ_ϕ is the viscous stress in the ϕ -direction as explained above.

The last conservation equation to consider is that for energy per unit area within the SL. This is composed of many pieces, the first being kinetic energy,

$$E_{\text{KE}} = \frac{1}{2} (v_\theta^2 + v_\phi^2) y. \quad (18)$$

The gravitational potential energy is

$$E_{\text{grav}} = \int_0^h \rho g_{\text{eff}} z dz = \frac{4}{5} \frac{g_{\text{eff}}}{g_{\text{eff}} - g_{\text{rad}}} \frac{kTy}{\mu m_p}. \quad (19)$$

The internal energy of the gas is

$$E_{\text{gas}} = \frac{3}{2} \int_0^h \frac{\rho kT}{\mu m_p} dz = \frac{6}{5} \frac{kTy}{\mu m_p}, \quad (20)$$

and the radiative energy is

$$E_{\text{rad}} = \int_0^h a T^4 dz = \frac{12}{5} \frac{g_{\text{rad}}}{g_{\text{eff}} - g_{\text{rad}}} \frac{kTy}{\mu m_p}. \quad (21)$$

The total radially integrated energy density is then $E_{\text{tot}} = E_{\text{KE}} + E_{\text{grav}} + E_{\text{gas}} + E_{\text{rad}}$. With this we express energy conservation as

$$\begin{aligned} \frac{\partial}{\partial t} (2\pi R E_{\text{tot}} \cos \theta) + \frac{1}{R} \frac{\partial}{\partial \theta} \left[2\pi R v_\theta \cos \theta \left(E_{\text{tot}} + \int_0^h P dz \right) \right] \\ = -2\pi R F \cos \theta, \end{aligned} \quad (22)$$

where the extra term added to the advected energy density is the radially integrated work that is done as fluid elements move higher in latitude. This expression can be simplified to give

$$\begin{aligned} R \cos \theta \frac{\partial E_{\text{tot}}}{\partial t} + \frac{\partial}{\partial \theta} \left[v_\theta \cos \theta \left(E_{\text{tot}} + \int_0^h P dz \right) \right] \\ = -R F \cos \theta. \end{aligned} \quad (23)$$

Equations (9), (11), (17), and (23) must now be solved to find the properties of the SL.

3.2. Taking the Steady State Limit

As in IS99 we solve the SL equations in the steady state limit ($\partial/\partial t = 0$) which greatly simplifies the solutions because θ is the only independent variable. To be a valid approximation, we require a sink for the accreted material at some latitude above the equator. The material near the equator moves in latitude rather quickly with $v_\theta \sim 10^5 - 10^6$ cm s⁻¹ (as we show in §4) and thus passes through the SL on a timescale of tens of seconds. Above this region the solutions show a long, deep minimum in v_θ for most of the star where $v_\theta \sim 10^4$ cm s⁻¹. This means that fluid still moving higher in latitude can only reach the pole on a timescale of $\sim 10^4$ s. At this point the fluid will have lost its azimuthal velocity, dissipated its high internal energy, and have an entropy set by the underlying WD luminosity. This means that long before the fluid has time to reach the pole it will mix with the slowly downward advecting fluid of the WD surface and thus be part of the WD. Recent theoretical calculations (Townsend & Bildsten 2003) and observations (Sion 1999) show that accreting WDs have effective temperatures $T_{\text{eff}} \approx (1-3) \times 10^4$ K. At a latitude at which the SL has reached a similar T_{eff} and has $v_\phi \approx 0$ we therefore set a sink where we stop our integrations.

The steady state assumption implies that continuity is set by the accretion rate, so that integrating equation (9) results in

$$\frac{1}{2} \dot{M} = 2\pi R y v_\theta \cos \theta. \quad (24)$$

We use $y v_\theta \cos \theta = \text{constant}$ and the steady state approximation to simplify the other conservation equations. Equation (11) becomes

$$\begin{aligned} y v_\theta \cos \theta \frac{dv_\theta}{d\theta} + \frac{4}{5} \cos \theta \frac{d}{d\theta} \left[\frac{g_{\text{eff}}}{g_{\text{eff}} - g_{\text{rad}}} \frac{kTy}{\mu m_p} \right] \\ = -R \tau_\phi \cos \theta - y v_\phi^2 \sin \theta. \end{aligned} \quad (25)$$

whereas equation (17) is rewritten

$$y v_\theta \cos \theta \frac{dv_\phi}{d\theta} = -R \tau_\phi \cos \theta + y v_\theta v_\phi \sin \theta. \quad (26)$$

Equation (23) is simplified to

$$\begin{aligned} y v_\theta \cos \theta \frac{d}{d\theta} \left[\frac{v_\theta^2 + v_\phi^2}{2} + \frac{2}{5} \frac{7g_{\text{eff}} + 3g_{\text{rad}}}{g_{\text{eff}} - g_{\text{rad}}} \frac{kT}{\mu m_p} \right] \\ = -R F \cos \theta. \end{aligned} \quad (27)$$

Rewriting equations (25), (26), and (27) in terms of the three dependent variables, v_θ , v_ϕ , and T we get,

$$\begin{aligned} v_\theta^2 \frac{dv_\theta}{d\theta} + \frac{4}{5} v_\theta^2 \cos \theta \frac{d}{d\theta} \left[\frac{g_{\text{eff}}}{g_{\text{eff}} - g_{\text{rad}}} \frac{kT}{\mu m_p} \right] \\ = -F_\theta - F_{\text{cen}}, \end{aligned} \quad (28a)$$

$$v_\theta v_\phi \frac{dv_\phi}{d\theta} = -F_\phi + F_{\text{cen}}, \quad (28b)$$

$$\begin{aligned} v_\theta^2 \frac{dv_\theta}{d\theta} + \frac{2}{5} v_\theta \frac{d}{d\theta} \left[\frac{7g_{\text{eff}} + 3g_{\text{rad}}}{g_{\text{eff}} - g_{\text{rad}}} \frac{kT}{\mu m_p} \right] \\ = F_\phi - F_{\text{cen}} - E_{\text{rad}}, \end{aligned} \quad (28c)$$

where the terms appearing on the right sides are: the frictional dissipations in the ϕ - and θ -directions,

$$F_\theta \equiv \alpha \frac{R}{h} v_\theta^2 \sqrt{v_\theta^2 + v_\phi^2}, \quad (29)$$

$$F_\phi \equiv \alpha \frac{R}{h} v_\phi^2 \sqrt{v_\theta^2 + v_\phi^2}, \quad (30)$$

where $h = P/(\rho g_{\text{eff}}) = kT/[\mu m_p(g_{\text{eff}} - g_{\text{rad}})]$ is the pressure scale height, the centrifugal term,

$$F_{\text{cen}} \equiv v_\theta v_\phi^2 \tan \theta, \quad (31)$$

and the radiative dissipation

$$E_{\text{rad}} \equiv \frac{RF}{y} = R g_{\text{rad}} v_\theta \frac{\dot{M}_{\text{Edd}}}{M} \cos \theta, \quad (32)$$

where $\dot{M}_{\text{Edd}} \equiv 4\pi R c/\kappa$ is the Eddington limit (with no rotation). In Appendix B we show how to solve equations (28a)–(28c) for each of the derivatives of the dependent variables to assist numerical integration.

4. SOLVING FOR THE SPREADING LAYER PROPERTIES

We now solve equations (28a)–(28c) by integrating from the equator toward the pole and halting integration once the sink has been reached. There are three boundary conditions at the equator for each of the dependent variables: $v_{\theta,0}$, $v_{\phi,0}$, and T_0 . Furthermore, we need an initial angle at which to begin our integrations, θ_0 . In §4.1 we consider the range of values appropriate for each of these variables, and show that because the accretion rates are so much less than the Eddington limit, the integrations naturally attract toward solutions where local viscous dissipation is approximately balanced by local radiative cooling. In §4.2 we analytically consider the differential equations to gain some intuition before considering the numerical results, including showing how θ_{SL} changes with \dot{M} and α . In §4.3 we present the full numerical solutions with descriptions of the important SL properties.

4.1. Boundary Conditions at the Equator

We begin by assuming that the accretion disk can be approximated by a standard, thin Shakura-Sunyaev disk. Using the disk height from Shakura & Sunyaev (1973; in the limit of gas pressure much greater than radiation pressure and using Kramer’s opacity) and dividing by R we find the disk subtends an angle at the WD surface of

$$\theta_{\text{disk}} = 1.5 \times 10^{-2} \alpha_{\text{disk}}^{-1/10} \dot{M}_{18}^{3/20} M_1^{-3/8} R_9^{1/8}, \quad (33)$$

where α_{disk} is the viscosity parameter for the accretion disk expected when the disk is actively accreting, $\dot{M}_{18} \equiv \dot{M}/(10^{18} \text{ g s}^{-1})$, $M_1 \equiv M/M_\odot$, $R_9 \equiv R/(10^9 \text{ cm})$, and we set the factor $[1 - (r/R)^{-1/2}] \approx 1$. We have chosen a rather high accretion rate for normalization because this is the regime where the SL will have the most observational impact. The material which comes in from the disk and subsequently spreads over the star must then start at an angle $\theta_0 \lesssim \theta_{\text{disk}}$. We therefore use a starting angle for integrations of $\theta_0 \approx 10^{-3}$. In cases where the spreading angle is comparable or less than θ_{disk} we say that spreading is negligible and most of the dissipated energy is radiated back into the disk. For the initial azimuthal velocity we use $v_{\phi,0} = 0.99 v_K$ so that the accreted material is moving in nearly Keplerian orbits when it reaches the star. This leaves two parameters to determine, $v_{\theta,0}$ and T_0 .

The initial temperature of the SL is set using the disk’s midplane temperature close to the WD. This is found from Shakura & Sunyaev (1973) to be

$$T_{\text{disk}} = 3.6 \times 10^5 \text{ K } \alpha_{\text{disk}}^{-1/5} \dot{M}_{18}^{3/10} M_1^{1/4} R_9^{-3/4}, \quad (34)$$

Finally, we must set the value of $v_{\theta,0}$. To see that there is a preferred value for this, consider setting $v_{\phi,0}$, T_0 , and θ_0 using the description above. We then perform a number of integrations,

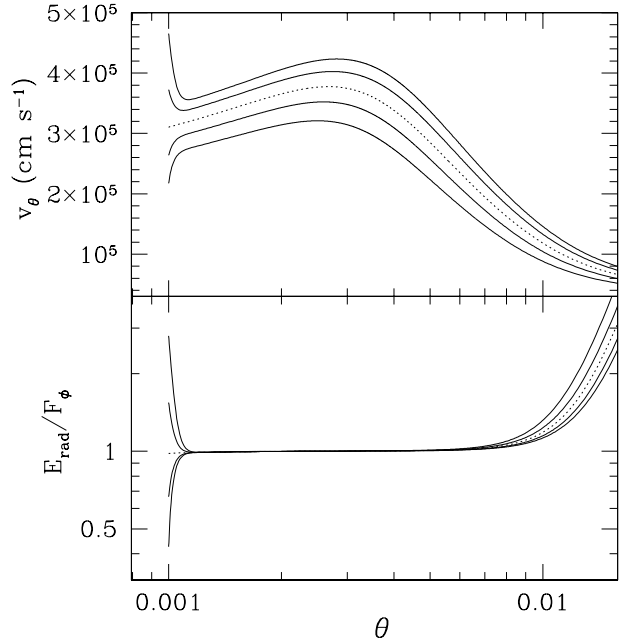


FIG. 2.— A number of sample integrations used to constrain the boundary condition at the equator. For all of the integrations we fix the values of $\theta_0 = 10^{-3}$, $v_{\phi,0} = 0.99 v_K$, $\alpha = 10^{-3}$, $\alpha_{\text{disk}} = 0.1$, and $\dot{M} = 3 \times 10^{17} \text{ g s}^{-1}$, for a white dwarf with $M = 0.6 M_\odot$ and $R = 9 \times 10^8 \text{ cm}$. T_0 is fixed using equations (34). Only $v_{\theta,0}$ is slightly different each time. Looking at the top panel it is clear that there is one preferred solution for v_θ (dotted line). The bottom panel shows the ratio E_{rad}/F_ϕ for the same set of integrations. Comparing the two panels, we see that this preferred solution corresponds to $E_{\text{rad}} \approx F_\phi$.

keeping all boundary values fixed while slightly varying $v_{\theta,0}$ each time. The results of these integrations are shown in Figure 2. In the top panel we see that the v_θ is naturally attracted toward a specific solution.

To find out the physical meaning behind this preferred solution, we consider these same integrations, instead following the ratio E_{rad}/F_ϕ , in the bottom panel of Figure 2. This ratio reflects how efficiently the system is locally radiating the energy dissipated from friction. If $E_{\text{rad}} < F_\phi$ then there must be advection because there is more local viscous heating than can be radiated away. On the other hand, if $E_{\text{rad}} > F_\phi$ the material loses internal energy because it is radiating so efficiently. (We can ignore F_θ because it is so much less than F_ϕ .) Comparing the top and bottom panels, we see that the asymptotic solution found for v_θ appears to correspond to the case when initially $E_{\text{rad}} = F_\phi$, which is when all of the viscous dissipation is being radiated away locally. To investigate further, we take a closer look at E_{rad}/F_ϕ in the top panel of Figure 3. This shows that in fact the attracting solution is $E_{\text{rad}} \lesssim F_\phi$, which means that a small amount of advection must take place. In the bottom panel of Figure 3 we see that the actual ratio depends on the accretion rate and that the higher the accretion rate is, the more advection takes place. With this information in hand, we then use $E_{\text{rad}} \lesssim F_\phi$ to get a closed set of equations so that the SL can be solved uniquely for a given \dot{M} and α (see Appendix C for additional details).

This boundary condition is different than the NS case studied by IS99 where it was found that the solutions are attracted toward the Eddington limit (i.e., $g_{\text{eff}} = g_{\text{rad}}$) and there is a great deal of advection. The differences between these results highlights the two limits of SL solutions. In the case of NSs, the

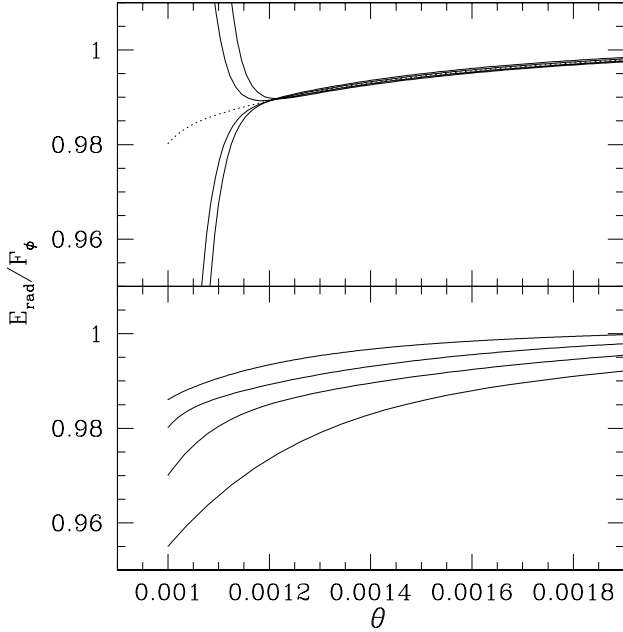


FIG. 3.— The top panel shows the same integrations as in Figure 2, but focusing near the equator. This shows that the actual asymptotic solution has $E_{\text{rad}} \lesssim F_{\phi}$, so that there is naturally a small amount of advection taking place. The bottom panel shows that solutions for accretion rates of 10^{17} , 3×10^{17} , 5×10^{17} , and 10^{18} g s^{-1} (from top to bottom) with all other values the same as in Figure (2). All solutions show $E_{\text{rad}} \lesssim F_{\phi}$ and furthermore, this inequality increases with higher accretion rate. As the accretion rate increases toward the Eddington limit we expect a great deal of advection as found by Inogamov & Sunyaev (1999) for the neutron star case.

local accretion rate through the disk is much closer to the Eddington rate making advection important. The low \dot{M} limit is the case of WDs considered here where radiation pressure is negligible so that little advection takes place. A similar regime likely exists for NSs at low accretion rates as well. In Figure 4 we show the initial latitudinal velocity, $v_{\theta,0}$, using the condition $E_{\text{rad}} = F_{\phi}$, along with $g_{\text{eff}} = g_{\text{rad}}$. At low accretion rates the two conditions are fairly different and the WD SL solutions are shown to have little advection and differ greatly from the NS case. As the accretion rate increases, the two conditions asymptote together and the WD solutions become more like the NS case. For boundary values at the right of the maximum in $v_{\theta,0}$ much more advection is seen in the solutions.

Given the prescription described above there is still an additional constraint for the values \dot{M} and α to be consistent with our plane parallel model which assumes that $h \ll R$. Substituting the boundary condition that $E_{\text{rad}} = F_{\phi}$ into $h < R$ provides the constraint

$$\alpha \lesssim 10^{-2} \alpha_{\text{disk}}^{3/5} \dot{M}_{18}^{-9/10} M_1^{-5/4} R_9^{7/4}. \quad (35)$$

This shows that at high \dot{M} , or when there is a lot of viscous dissipation because of a high α , it is possible that the SL will expand so that $h \approx R$. This case is interesting for some high \dot{M} systems (such as symbiotic binaries which can have $\dot{M} \approx 10^{20} \text{ g s}^{-1}$), so although outside the scope of this paper, such regions of parameter space should be studied in the future.

4.2. Analytic Estimates

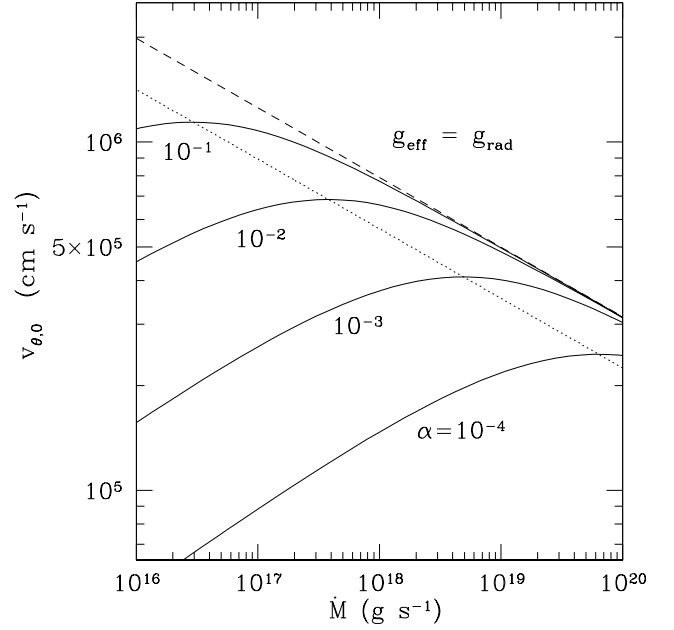


FIG. 4.— The initial latitudinal velocity, $v_{\theta,0}$, versus accretion rate, using the boundary condition that $E_{\text{rad}} = F_{\phi}$ (solid lines). The dashed line denotes the Eddington limit $g_{\text{eff}} = g_{\text{rad}}$ and the dotted lines pass through the maximum value $v_{\theta,0}$ can attain for a given viscosity, α . Solutions taken from the left of the dotted line show little advection and a strong attraction toward the $E_{\text{rad}} = F_{\phi}$. Solutions using $v_{\theta,0}$ from the right of the dotted line show much more advection, similar to the case of neutron stars investigated by Inogamov & Sunyaev (1999).

As a first attempt at approximating the spreading angle, θ_{SL} , one might guess that it is given by geostrophic balance (when the pressure gradient in the latitudinal direction is balanced by the Coriolis force pushing back toward the equator). This can be found using conservation of momentum in the θ -direction, equation (25). Approximating $v_{\theta} \ll v_{\phi}$, $g_{\text{rad}} \ll g_{\text{eff}}$, and $\theta \ll 1$, this results in

$$\frac{d}{d\theta} \frac{kTy}{\mu m_p} \approx -y v_{\phi}^2 \theta. \quad (36)$$

This then gives θ_{SL} approximately as

$$\theta_{\text{SL}} \approx \left(\frac{kT}{\mu m_p} \right)^{1/2} v_{\phi}^{-1}. \quad (37)$$

This may provide the correct estimate when friction is negligible, but it gives the incorrect scalings for the case we are considering here where friction is the primary agent for slowing the flow.

Using this insight, we now derive approximate solutions, instead assuming that conservation of ϕ -momentum is controlling the flow. This will illuminate the general features of the SL and provide power law scalings consistent with numerical integrations. We first must estimate the size and scaling of v_{θ} . Setting $E_{\text{rad}} = F_{\phi}$ near the equator we find

$$R g_{\text{rad}} v_{\theta} \frac{\dot{M}_{\text{Edd}}}{\dot{M}} \approx \alpha \frac{R}{h} v_{\phi}^2 \sqrt{v_{\theta}^2 + v_{\phi}^2} \approx \alpha \frac{R}{h} v_{\phi}^3. \quad (38)$$

Solving equation (38) for v_{θ} gives the approximate latitudinal velocity in the SL. Using equation (34) to set the temperature we find

$$v_{\theta,\text{SL}} = 2.1 \times 10^6 \text{ cm s}^{-1} \alpha_{\text{disk}}^{1/2} \alpha_3^{1/2} \dot{M}_{18}^{1/4} M_1^{5/8} R_9^{-7/8}, \quad (39)$$

where $\alpha_3 \equiv \alpha/10^{-3}$.

To understand the effect of friction on setting θ_{SL} we use conservation of momentum in the ϕ -direction, equation (28b), which near the equator is

$$v_\theta v_\phi \frac{dv_\phi}{d\theta} = -F_\phi = -\alpha \frac{R}{h} v_\phi^3. \quad (40)$$

We can then estimate

$$\theta_{\text{SL}} \approx \frac{h v_\theta v_\phi}{R \alpha v_\phi^2}. \quad (41)$$

This gives the simple explanation that θ_{SL} is set by two factors: (1) the pressure gradient in the latitudinal direction (the first term), and (2) the competition between ϕ -momentum fluxing in the θ -direction, $v_\theta v_\phi$, and dissipation of ϕ -momentum due to viscous stress, αv_ϕ^2 . This scaling is different than the results of IS99 who found that the spreading flow adjusts itself so as to radiate everywhere at close to the local Eddington rate, and thus their θ_{SL} depends only on the ratio $\dot{M}/\dot{M}_{\text{Edd}}$. At much less than the Eddington rate, equation (41) shows that θ_{SL} is proportional to h and therefore highly dependent on the initial properties of the material when it first reaches the WD equator. We can find the functional relationship between v_ϕ and θ by assuming that v_θ and T are constant and integrating equation (40). Setting $g_{\text{eff}} = GM/R^2 - v_\phi^2/R$ and using $\theta_0 \approx 0$ this results in

$$\theta = \frac{1}{\alpha} \frac{kT}{\mu m_p v_K^2} \frac{v_\theta}{v_K} \times \left(\frac{v_K}{v_\phi} - \frac{v_K}{v_{\phi,0}} + \log \frac{\sqrt{1-v_\phi/v_K}}{\sqrt{1+v_\phi/v_K}} - \log \frac{\sqrt{1-v_{\phi,0}/v_K}}{\sqrt{1+v_{\phi,0}/v_K}} \right) \quad (42)$$

Figure 5 shows this result plotted alongside the numerical solutions found in the next section. The analytic estimate shows only qualitative agreement, which is not surprising given the crudeness of the estimates made, namely that both v_θ and T are constant. We estimate the spreading angle, θ_{SL} , by assuming that $v_\phi \approx 0.1 v_K$ at the end of the spreading. In the limit of $v_{\phi,0} \approx v_K$ we find

$$\theta_{\text{SL}} = \frac{1}{\alpha} \frac{kT}{\mu m_p v_K^2} \frac{v_\theta}{v_K} \left(9 + \frac{1}{2} \log \frac{18/11}{1-v_{\phi,0}/v_K} \right). \quad (43)$$

This result has a singularity at $v_{\phi,0} = v_K$ (which it must because material moving at the Keplerian velocity will not settle onto the WD), but even for values $v_{\phi,0} \lesssim v_K$ this last term is only of order a few and has little effect on this angle estimate. Substituting v_θ and T by using equations (39) and (34), and setting $v_{\phi,0} = 0.99 v_K$ we find

$$\theta_{\text{SL}} = 2.4 \times 10^{-2} \alpha_{\text{disk}}^{3/10} \alpha_3^{-1/2} \dot{M}_{18}^{11/20} M_1^{-5/8} R_9^{-1/8}. \quad (44)$$

The scalings predicted by equation (44) are consistent with those found performing the numerical integrations (as we describe in the following section). This derivation shows that the change in v_ϕ and the value of θ_{SL} are mainly dictated by viscous dissipation. Using $(d/dt)(v_\phi) = -\alpha \rho v_\phi^2$, we estimate a timescale for spreading of

$$t_{\text{SL}} = h/(\alpha v_\phi) \approx 50 \text{ s } \alpha_{\text{disk}}^{-1/5} \alpha_3^{-1} \dot{M}_{18}^{3/10} M_1^{-5/4} R_9^{7/4}. \quad (45)$$

This timescale is extremely short and mainly due to the small amount of material which is in the SL at any given time. This implies that if accretion decreases dramatically (such as following a dwarf nova outburst) the hot belt around the equator

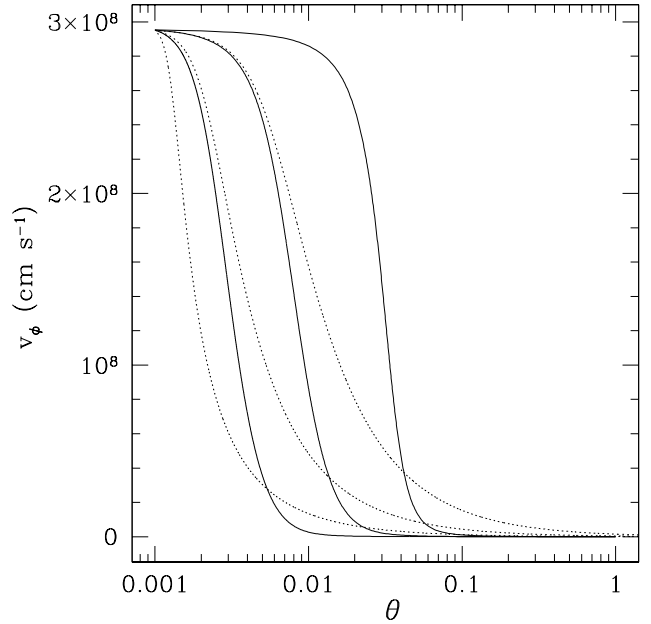


FIG. 5.— A comparison between the numerical integrations (solid lines) with the analytic estimate given by equation (42) (dotted lines). Accretion rates of $\dot{M} = 10^{17}$, 10^{18} , and 10^{19} g s^{-1} are shown (from left to right), all with $\alpha = 10^{-3}$, $\alpha_{\text{disk}} = 0.1$, $M = 0.6 M_\odot$, and $R = 9 \times 10^8 \text{ cm}$. Though quantitatively different, the two results are qualitatively similar and both predict similar spreading angles at $v_\phi = 0.1 v_K \approx 3 \times 10^7 \text{ cm s}^{-1}$. At higher accretion rates the solutions differ more because the analytic estimate ignores radiation pressure effects.

will spread fairly quickly over the WD surface and not be visible days or even hours later.

Since at low accretion rates $\theta_{\text{SL}} \lesssim \theta_{\text{disk}}$, the spreading material will most likely be obscured by the disk, making direct observations of the SL difficult. Setting $\theta_{\text{SL}} = \theta_{\text{disk}}$ we solve for the critical \dot{M} at which the SL will extend above the disk,

$$\dot{M}_{\text{crit}} > 3.7 \times 10^{17} \text{ g s}^{-1} \alpha_{\text{disk}}^{3/2} \alpha_3^{5/4} M_1^{15/8} R_9^{5/8}. \quad (46)$$

The large value of this accretion rate implies that the effects of the SL may only be seen in a select number of systems where a high \dot{M} occurs such as dwarf novae, symbiotic binaries, and supersoft sources. Lower accretion rate sources must still have dissipation occurring at the interface between the disk and WD surface, but the radiation created in these cases is most likely absorbed and re-radiated by the accretion disk. We discuss all of these issues in more detail in §5.

Using the results from above we find that the local flux in the SL is approximately,

$$F_{\text{SL}} = 1 \times 10^{17} \text{ erg cm}^{-2} \text{ s}^{-1} \alpha_{\text{disk}}^{-3/10} \alpha_3^{1/2} \dot{M}_{18}^{9/20} M_1^{13/8} R_9^{-23/8} \quad (47)$$

Multiplying by the area of the spreading zone which is $4\pi R^2 \sin \theta_{\text{SL}} \approx 4\pi R^2 \theta_{\text{SL}}$ provides the luminosity. Comparing equations (44) and (47) we find that $L \propto \dot{M}$ and independent of both α and α_{disk} as it must be since these are free parameters. The value of the luminosity is consistent with standard energy conservation arguments, $L = G\dot{M}\dot{M}/(2R)$. This means that luminosity alone will not tell us whether a SL is present. A better test would be a study of the emitting area and T_{eff} . The emitting area scales like θ_{SL} which is expressed above. The T_{eff} is given by the flux so that from equation (47) we

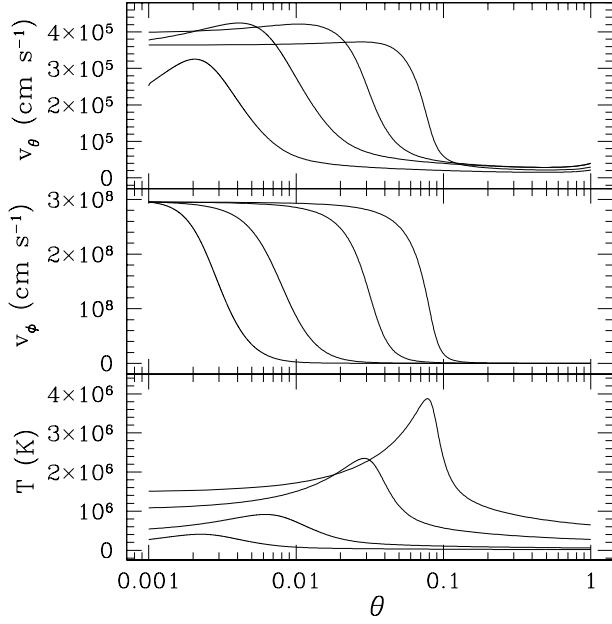


FIG. 6.— The velocities and temperature of the spreading layer for a white dwarf with $M = 0.6M_{\odot}$ and $R = 9 \times 10^8$ cm, with $\alpha = 10^{-3}$ and $\alpha_{\text{disk}} = 0.1$. From left to right the accretion rates are 10^{17} , 10^{18} , 10^{19} and 3×10^{19} g s $^{-1}$.

find

$$T_{\text{eff,SL}} = 2 \times 10^5 \text{ K } \alpha_{\text{disk}}^{-3/40} \alpha_3^{1/8} \dot{M}_{18}^{9/80} M_1^{13/32} R_9^{-23/32}. \quad (48)$$

This value is not so different than what would have been approximated from BL arguments (for example see Frank, King & Raine 2002). This is not surprising since even if the SL increases the emitting area by a factor of 10, the effective temperature would only change by a factor of 1.8. The best test to see if spreading is taking place is to follow how T_{eff} changes with \dot{M} . The SL model shows that T_{eff} will change much more gradually than if the radiating area on the WD is fixed (which would predict $T_{\text{eff}} \propto \dot{M}^{1/4}$).

4.3. Numerical Solutions

We now present the full numerical solutions of equations (28a)–(28c). These confirm the general estimates made in the previous section and also provide additional details that cannot be investigated analytically. For these integrations we use the fiducial values of $M = 0.6M_{\odot}$, $R = 9 \times 10^8$ cm, and $\alpha_{\text{disk}} = 0.1$. The composition of the accreting material is assumed to be solar so that $\mu = 0.62$ and $\kappa = 0.34 \text{ cm}^2 \text{ g}^{-1}$.

First we set our boundary value for T_0 using the temperature of equation (34), and then we set $v_{\theta,0}$ by using the condition that $E_{\text{rad}} \lesssim F_{\phi}$. The integrations are then performed on the three coupled differential equations as derived in Appendix B from equations (28a)–(28c). In Figures 6 and 7 we plot the properties of the SL for $\alpha = 10^{-3}$ and a range of accretion rates. At low accretion rates ($\dot{M} \approx 10^{17} - 10^{18}$ g s $^{-1}$) we find the numerical integrations result in values close to what was approximated analytically in the previous section. At the higher accretion rates ($\dot{M} \gtrsim 10^{19}$ g s $^{-1}$) more advection takes place, resulting in solutions which look similar to what IS99 found for neutron stars. Most notably, the temperature profiles show large peaks at high latitudes due to energy being advected away from the equator and deposited higher up on

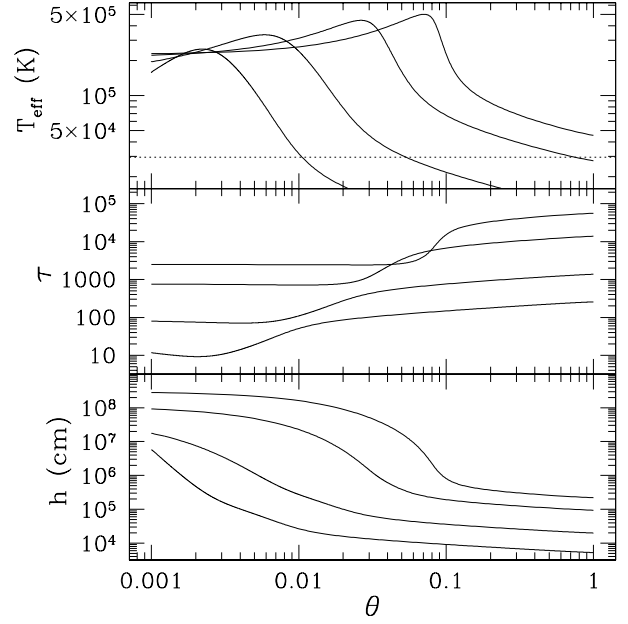


FIG. 7.— The effective temperature, optical depth, and pressure scale height of the spreading layer, using the same parameters as in Figure 6. The dotted line shows $T_{\text{eff}} = 3 \times 10^4$ K, a fiducial temperature for the underlying accreting white dwarf.

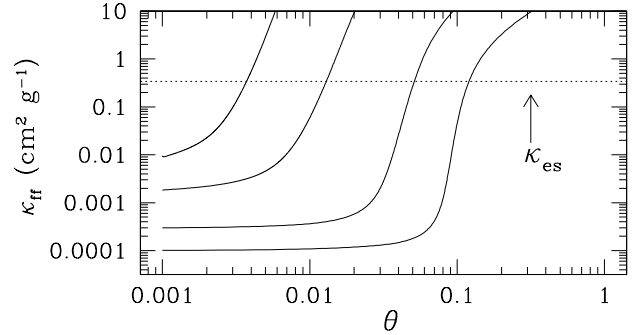


FIG. 8.— The free-free opacity, κ_{ff} , calculated using the properties of the spreading layer solutions, using the same parameters as in Figure 6. This can be compared to the electron scattering opacity, $\kappa_{\text{es}} = 0.34 \text{ cm}^2 \text{ g}^{-1}$ (dotted line), to see that the opacity is correctly approximated for the majority of the spreading layer, especially in the regions which provide the majority of the flux.

the star. In Figure 7 we denote the fiducial T_{eff} expected for the underlying accreting WD. Comparing this and Figure 6 shows that once the SL has come into thermal balance with the underlying WD, the SL is also rotating with the WD ($v_{\phi} \approx 0$). The optical depth is shown to always be much greater than unity, so that our assumptions of a radiation pressure acting in our one-zone envelope and a true T_{eff} are valid. At high accretion rates the scale height becomes comparable to R , showing the limit of the plane parallel model. Our viscous stress parametrization becomes questionable at low accretion rates ($\dot{M} \lesssim 10^{17}$ g s $^{-1}$) when the latitudinal shear is much greater than the shear between the SL and underlying WD (because $R\theta_{\text{SL}} < h$). Qualitatively, this does not change the important result that most or all of the SL dissipation happens within the width of the accretion disk at these accretion rates. Figure 8

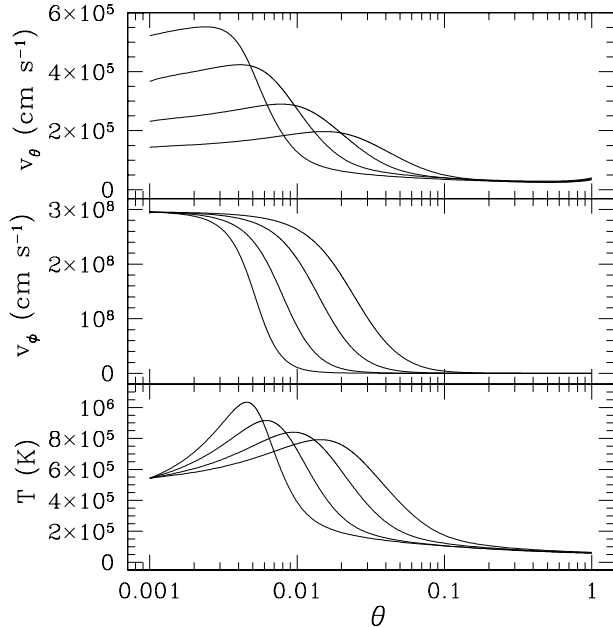


FIG. 9.— The velocities and temperature of the spreading layer for a white dwarf with $M = 0.6M_{\odot}$ and $R = 9 \times 10^8$ cm, with $\dot{M} = 10^{18}$ g s $^{-1}$ and $\alpha_{\text{disk}} = 0.1$. From left to right the values of α are 3×10^{-3} , 10^{-3} , 3×10^{-4} , and 10^{-4} .

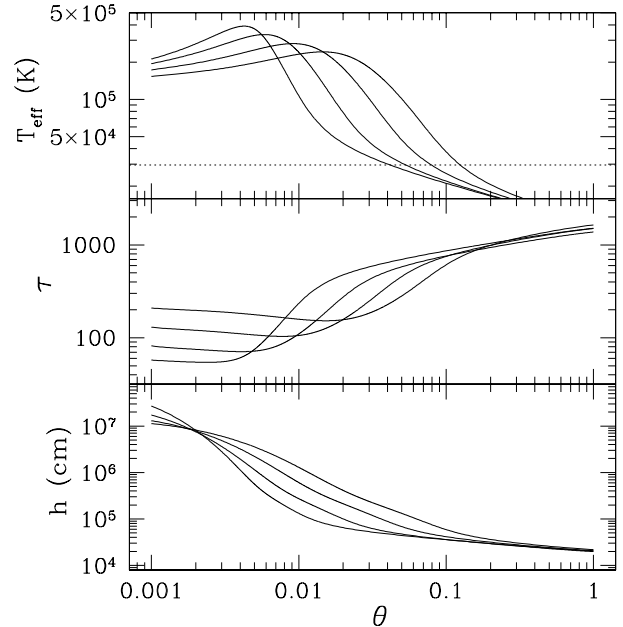


FIG. 10.— The effective temperature, optical depth, and pressure scale height of the spreading layer, using the same parameters as in Figure 9. Viscous stress decreases from left to right. The dotted line shows $T_{\text{eff}} = 3 \times 10^4$ K, a fiducial temperature for the underlying accreting white dwarf.

shows the free-free opacity, calculated from the solutions that are found using a constant electron scattering opacity. For all solutions, the free-free opacity is small in the hot portions of the SL. This gives some confidence that T_{eff} over this region is accurate, because the majority of the flux is radiated here. Unfortunately, our opacity assumption always breaks down in regions where the SL is cool which makes any spectrum calculation based on this model somewhat dubious. In Figures 9 and 10 we show that the properties of the SL can vary depending on the value of the viscosity.

Figure 11 summarizes the key feature of the SL which is how the spreading angle (and thus the radiating area) changes with accretion rate. At low accretion rates the scaling is consistent with what was found analytically, equation (44). Figure 11 reinforces the result that high accretion rates are needed for any hope of appreciable spreading to take place. It is important to note that even when the accretion disk covers the main portion of the SL, the SL may still have some observational impact depending on the viewing angle of the WD and how far the contrast in T_{eff} extends (see Figures 7 and 10).

5. INITIAL COMPARISONS TO OBSERVATIONS

From the analysis in §4, it is qualitatively clear that the SL is best observed in high accretion rate systems so that it is not obscured by the accretion disk or its winds. This suggests that the best candidates to show a SL are dwarf novae, symbiotic binaries, and supersoft sources. We now review the current observations of these accreting WDs in the EUV and soft X-rays.

5.1. Dwarf Nova Outbursts

There have been a number of observations of dwarf novae in outburst or superoutburst using the *Extreme Ultraviolet Explorer (EUVE)*, including those of SS Cyg (Mauche, Raymond & Mattei 1995; Wheatley, Mauche & Mattei 2003,

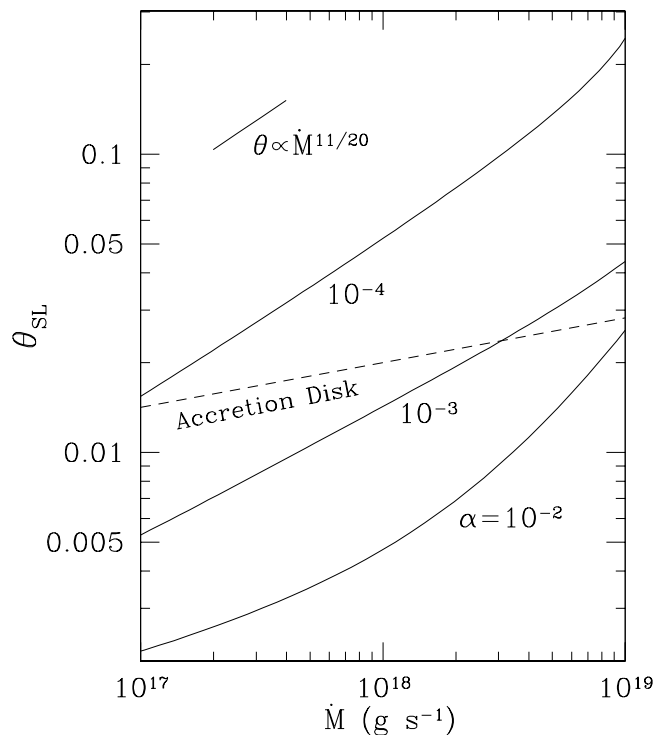


FIG. 11.— The spreading angle, θ_{SL} , versus accretion rate for a white dwarf with $M = 0.6M_{\odot}$ and $R = 9 \times 10^9$ cm and three different viscous stress parameters. The spreading angle is defined as the angle at which $v_{\phi} = 0.1v_K$. At low accretion rates the scaling with \dot{M} is fairly consistent with what is expected from an analytic approximation which gives $\theta_{\text{SL}} \propto \dot{M}^{11/20}$. This also shows that high accretion rates are needed for the spreading layer to extend beyond the angle made by a Shakura-Sunyaev disk, equation (33) (dashed line).

hereafter WMM03), U Gem (Long et al. 1996), VW Hyi (Mauche 1996) and OY Car (Mauche & Raymond 2000). Mauche, Mattei & Bateson (2001) provides a review of many of these objects.

WMM03 provide an especially interesting observation of an outburst of SS Cygni studied in the optical by The American Association of Variable Star Observers (AAVSO), in the X-rays by the *Rossi X-ray Timing Explorer* (RXTE), and in the EUV using *EUVE*. The observations show a complete optical light curve, following the burst over ~ 12 days. The X-rays show two small bursts of activity, the first coming ~ 1.5 days after the initial rise in the optical and the second coming near the end of the outburst. In between there is emission in the EUV. The correlations between these three bands are consistent with what is expected by the standard dwarf nova picture. The outburst begins once the disk is in the high state, starting the rise in optical, and then proceeds from the outside of the disk in. Once material begins accreting onto the WD it is initially optically thin, and thus radiates in the X-rays at a temperature given by the virial temperature of the accreting gas (Pringle & Savonije 1979; Tytenda 1981; Narayan & Popham 1993). This provides the initial ~ 1.5 days of X-rays. Once the material becomes optically thick, it radiates in the EUV for most of the remainder of the burst (Pringle 1977; Tytenda 1977; Popham & Narayan 1995). Finally, at the end, the material becomes optically thin one last time, radiating a little more in the X-rays before the outburst ceases.

Qualitatively, a similar picture is also expected for a SL, even though the calculations we perform above only apply when the SL is optically thick. One might expect the SL to be important because of the large inferred accretion rates at the peak of the outburst ($\sim 10^{18} \text{ g s}^{-1}$). As discussed in §4.2, evidence that spreading is occurring requires studying the change in effective temperature with accretion rate. If the radiating area does not change with accretion rate then one expects $T_{\text{eff}} \propto \dot{M}^{1/4}$. On the other hand, since the area increases with \dot{M} for the SL we find $T_{\text{eff}} \propto \dot{M}^{9/80}$, equation (48). Figure 12 shows the count rate (which is proportional to luminosity) versus the hardness ratio (related to T_{eff}) taken from this observation by WMM03. Fit are the two power laws expected from a SL and a constant radiating area. Even though this does not show conclusively that the SL exists, this shows in principle the kind of test which needs to be done as data improves. Other observations of SS Cyg (such as Mauche, Raymond & Mattei 1995), also report a fairly constant hardness ratio during outburst even though the count rate changes by two orders of magnitude.

Another suggestive result by Mauche, Raymond & Mattei (1995) is the count rate in the EUV as compared with typical count rates in the optical for similar outbursts. If the former is assumed to represent the region up close to the WD and the latter the accretion disk, these observations suggest that the ratio of the two luminosities is $L_{\text{BL}}/L_{\text{disk}} \lesssim 0.07$. This is in stark contrast from $L_{\text{BL}}/L_{\text{disk}} \sim 1$ as expected from BL models. It is possible that because the SL only extends a small distance above the disk, much of the radiation from the SL is obscured by, or contained within, the accretion disk or its winds.

A much more complicated picture is provided by the superoutburst of the edge-on binary OY Car (Mauche & Raymond 2000). By comparing optical and EUV lightcurves during outburst they find that while the optical is eclipsed, the EUV shows no sign of being eclipsed. This calls into question

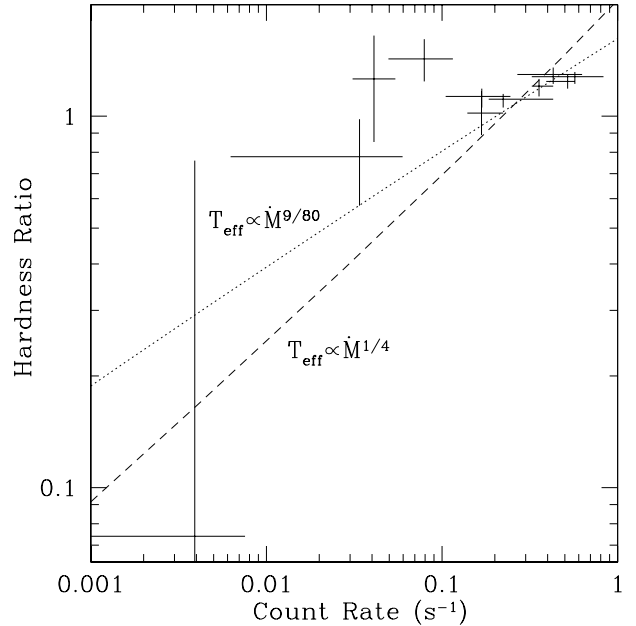


FIG. 12.— Hardness ratio versus count rate as measured during a dwarf nova outburst of SS Cyg by Wheatley, Mauche & Mattei (2003). The hardness ratio is defined as the ratio of counts between the the 72–95 Å band (excluding 76–80 Å) to the 95–130 Å band. Plotted over the data are the relations expected from the spreading layer (dotted line) and a model which has constant radiating area (dashed line). In each case the area is assumed to radiate like a blackbody and the Wein limit is used. The scaling between count rate and accretion rate is treated as a free parameter used to maximize the fit in each case. The spreading layer gives a shallower power law, as expected because its radiating area increases with accretion rate, but it provides only a slightly better fit to the data.

the assumption that the EUV is associated with a region near the WD and suggests that perhaps the EUV is from a much more extended region than previously thought. Good fits are made to the outburst spectrum by assuming that the radiation from both the BL and accretion disk are scattered into the observer's line of sight by an ionized accretion disk wind. These additional complications make it difficult to simply compare our SL with this or similar observation.

In a study of U Gem using the *Far Ultraviolet Spectroscopic Explorer* (FUSE), Froning et al. (2001) model the spectra both during outburst and in the decline afterwards in the far-ultraviolet. They find that the majority of the spectra during outburst is consistent with a steady state accretion disk with $\dot{M} = 4.6 \times 10^{17} \text{ g s}^{-1}$. This is close to the critical accretion rate found in equation (46) so that we might guess a SL is present. The accretion disk model underpredicts the observed spectra at short wavelengths ($< 950 \text{ Å}$), which is a sign of a missing hot component, perhaps the SL. Though suggestive, there is still more work to be done to determine whether a SL has been seen. It is not clear whether accretion disk model improvements would explain this difference. In the same study by Froning et al. (2001), they also look at U Gem a few days after the outburst peak when the luminosity is declining. They find that the spectra are very well fit by a WD model. They also attempt a fit which includes an additional hot belt on the WD, but they find that the improvement of the fit is negligible. This is long after the timescale we find for spreading, equation (45), so we do not expect to see a SL in this case.

In an observation of VW Hyi, Sion et al. (1996) use the *Hubble* Faint Object Spectrograph (FOS) to look at spectra a day after a dwarf nova outburst and ten days after a super outburst. In each case they compare spectral fits of a single WD model with the fits of a WD plus a hot belt, and for both observations they find that the latter model provides a better fit. From the solutions found for the SL in §4 it is surprising that the hot belt is still present on the WD this many days after outburst when the SL should have already spread over the star due to friction. Other observations by the same group (Huang et al. 1996a, 1996b) show similar, but less conclusive results.

5.2. Symbiotic Binaries and Supersoft Sources

Another promising candidate for showing a SL are symbiotic binaries. These are WDs which are accreting from the winds of red giants with $\dot{M} = 10^{17} - 10^{20} \text{ g s}^{-1}$, and they typically show a hot component which may or may not be coming from near the WD. Mürset, Nussbaumer, Schmid & Vogel (1991) review the characteristics of this hot component for a large number of systems, finding luminosities in the range $0.3L_{\odot} \lesssim L \lesssim 3.7 \times 10^4 L_{\odot}$ and effective temperatures around $5.5 \times 10^4 \text{ K} \lesssim T_{\text{eff}} \lesssim 2.1 \times 10^5 \text{ K}$. From these two quantities the radius associated with the emitting region can be estimated. This is typically $\sim 10^{10} \text{ cm}$, much larger than expected if the radiation were coming directly from the WD surface, which suggests the presence of a hot ionized nebula surrounding the WD. There are three systems listed in Mürset et al. (1991) which have features qualitatively different than most other symbiotic binaries; these are EG And, AG Dra, and CH Cyg. All three of these systems are underluminous in comparison with the other symbiotic binaries which implies a much smaller radius, closer to what is expected for WD. A May 1988 observation of CH Cyg resulted in an inferred radius of $1.4 \times 10^8 \text{ cm}$ which is even too small to be a WD. Though Mürset et al. (1991) argue this could be due to an incorrect distance measurement, it could also be a sign of the SL. Two of these systems show flickering in the optical (EG And and CH Cyg; Sokoloski, Bildsten & Ho 2001), which is a trait uncommon to symbiotics, but common to accreting CVs. This may point to disk accretion being present and thus also a SL.

Finally, supersoft sources are WD binaries with $\dot{M} \sim 10^{18} - 10^{20} \text{ g s}^{-1}$. At these high accretion rates accreted hydrogen on the WD surface is believed to be burning steadily (van den Heuvel et al. 1992; Heise, van Teeseling & Kahabka 1994) and this provides the large luminosity seen from these sources ($\sim 10^{37} - 10^{38} \text{ erg s}^{-1}$). The SL would appear at a significantly different T_{eff} from the WD surface because of the difference in emitting area. The problem with these systems is that the burning causes such high luminosities that the SL would be dwarfed in comparison. Current observations of supersoft sources do not have enough signal to show a SL and would require much more detailed models to correctly determine whether a SL is present.

6. DISCUSSION AND CONCLUSIONS

The SL model, first conceived by IS99, provides a new way of understanding the properties of newly accreted material and its interaction with the stellar surface. In this model the latitudinal direction is used as the independent variable, as opposed to standard BL models which follow how the disk changes near the star along the radial direction. This allows an investigation of the radiating area of the hot belt which forms near the equator, and it describes the properties of the

accreting material when it first comes into hydrostatic balance on the star. We have investigated the solutions of the SL model when applied to WDs, accreting in the range of $\dot{M} \sim 10^{17} - 10^{19} \text{ g s}^{-1}$. We find that the integrations for the spreading flow naturally attract toward solutions in which initially local radiative cooling balances local viscous dissipation. As the accretion rate gets higher, we find increasingly more advection in the flow, similar to the solutions for NSs investigated by IS99. The spreading angle on WDs is found to typically be $\theta_{\text{SL}} \approx 0.01 - 0.1$, depending on both the accretion rate and the viscosity. The SL has an effective temperature in the range of $(2 - 5) \times 10^5 \text{ K}$ with a pressure scale height of $10^7 - 10^8 \text{ cm}$.

To be clearly observed in actively accreting systems, the SL must extend to a large enough angle to be seen above the accretion disk. This requires the accretion rate to be high, $\dot{M} \gtrsim 10^{18} \text{ g s}^{-1}$, assuming that the accretion disk is similar to a thin Shakura-Sunyaev disk. The best candidates to show the SL are dwarf novae in outburst, supersoft sources, and symbiotic binaries. Current observations of the dwarf novae may be the best opportunity to see if spreading is actually occurring. The scaling of effective temperature with accretion rate is much weaker in the case of a SL because of the change in radiating area. At lower accretion rates, $\dot{M} \lesssim 10^{18} \text{ g s}^{-1}$, the SL will not spread far from the equator and most of the dissipated energy will radiate back into the accretion disk. Although this may make comparison between theory and observations difficult, because the SL cannot be seen directly, it may still have important consequences for the accretion disk structure and spectra.

The short timescale for spreading, $t_{\text{SL}} \sim 50 \text{ s}$, suggests that a hot belt around the WD equator will be difficult to see after an outburst because the hot material should spread over the WD surface quickly. This also means that mixing between freshly accreted material and much deeper layers appears difficult on accreting WDs. Rosner et al. (2001) and Alexakis et al. (2003) have argued that the mixing of recently accreted H/He with the underlying layer of C/O due to rotational shearing explains observations of CNO nuclei in the ejecta of nova. To have t_{SL} of order the accretion time ($\sim 10^3 \text{ yr}$) requires $\alpha \lesssim 10^{-11}$, so that the viscosity must be even less than what is estimated from microphysics (see Appendix A). This makes it difficult to imagine mixing via this mechanism all the way down to the C/O layers.

The initial calculations by IS99 and in this paper describe some of the general features of the SL model, a new area of investigation which will lead to further studies of how accreted material settles onto stars. This may include studying how differential rotation and angular momentum transfer affect the underlying stellar surface or the possibility of nonradial oscillations present in the SL. Spectral modeling of the SL, along comparisons with observations, may also help in identifying if and when spreading is present.

We thank Rashid Sunyaev for helpful and enthusiastic discussions about spreading, and Christopher Mauche for answering our questions about cataclysmic variable observations. We have also benefitted from conversations with Phil Arras, Philip Chang, Chris Deloye, Aristotle Socrates, and Dean Townsley. We thank the referee for a careful reading of this paper along with many helpful suggestions. This work was supported by the National Science Foundation under grants PHY99-07949 and AST02-05956 and by the Joint Institute for Nuclear Astrophysics through NSF grant PHY02-

APPENDIX

A. VISCOUS STRESS PARAMETRIZATION

In the derivation of the spreading differential equations we choose to parametrize τ in terms of a unitless constant, α , so that

$$\tau = \alpha \rho v^2. \quad (\text{A1})$$

We follow IS99 and estimate the values of α implied by possible ionic or radiative viscosities. In general the viscous stress is expected to be set by turbulence, so these estimates only provide a lower limit to α . The ion viscosity, ν_i , is related to the viscous stress by

$$\tau = \nu_i \rho \frac{\partial v}{\partial z} \approx \nu_i \rho \frac{v}{h}. \quad (\text{A2})$$

Using the ion viscosity of Spitzer (1965) we find $\nu_i \approx 2 \times 10^6 \text{ cm}^2 \text{ s}^{-1}$ (using typical values of the spreading layer solutions from §4). Equations (A1) and (A2) can be combined to find $\alpha \sim 10^{-10}$, which shows that this contribution can be ignored. We next consider the radiative viscosity, ν_r , which is given by

$$\tau = \nu_r \rho_r \frac{\partial v}{\partial z} \approx \nu_r \rho_r \frac{v}{h}, \quad (\text{A3})$$

where $\rho_r = aT^4/c^2$ is the radiation density. The radiative viscosity can be written as $\nu_r = \lambda c$, where λ is the photon mean free path given by $\lambda = 1/(\rho \kappa)$. We then solve for α and find it can be written in terms of three ratios as

$$\alpha = \frac{\rho_r \lambda c}{\rho h v} \sim 10^{-6}, \quad (\text{A4})$$

which is small due to $\rho_r/\rho \ll 1$. Though larger than the former value for α , this quick check shows that neither of these mechanisms are large enough to provide the viscosity needed to slow down the spreading material. We therefore assume that there is a turbulent viscosity which results in higher values of α and leave this as a free parameter. In IS99, this form of the viscous stress, equation (A1), is contrasted with the form typically used for accretion disks ($\tau = \alpha c_s h$, where c_s is the speed of sound; Shakura & Sunyaev 1973). The latter prescription for the viscous stress describes the friction between adjacent annuli of the layer and IS99 show that it is negligible as long as $h/R \ll 1$ (so that most of the free energy is at the SL/WD boundary).

B. REWRITING THE DIFFERENTIAL EQUATIONS FOR NUMERICAL INTEGRATION

To solve equations (28a)–(28c) numerically we must solve for each of the derivatives in terms of the dependent variables. This involves expanding the messy derivatives in equations (28a) and (28c). From equation (28a) we need

$$\begin{aligned} \frac{d}{d\theta} \left[\frac{g_{\text{eff}}}{g_{\text{eff}} - g_{\text{rad}}} \frac{kT/(\mu m_p)}{v_\theta \cos \theta} \right] &= \frac{g_{\text{eff}}}{g_{\text{eff}} - g_{\text{rad}}} \frac{1}{v_\theta \cos \theta} \frac{d}{d\theta} \frac{kT}{\mu m_p} - \frac{g_{\text{eff}}}{g_{\text{eff}} - g_{\text{rad}}} \frac{kT/(\mu m_p)}{v_\theta^2 \cos \theta} \frac{dv_\theta}{d\theta} + \frac{1}{g_{\text{eff}} - g_{\text{rad}}} \frac{kT/(\mu m_p)}{v_\theta \cos \theta} \frac{dg_{\text{eff}}}{d\theta} \\ &\quad - \frac{g_{\text{eff}}}{(g_{\text{eff}} - g_{\text{rad}})^2} \frac{kT/(\mu m_p)}{v_\theta \cos \theta} \frac{d}{d\theta} (g_{\text{eff}} - g_{\text{rad}}) + \frac{g_{\text{eff}}}{g_{\text{eff}} - g_{\text{rad}}} \frac{kT/(\mu m_p)}{v_\theta \cos \theta} \tan \theta. \end{aligned} \quad (\text{B1})$$

The individual derivatives in this expression are given by

$$\frac{dg_{\text{eff}}}{d\theta} = -\frac{2v_\theta}{R} \frac{dv_\theta}{d\theta} - \frac{2v_\phi}{R} \frac{dv_\phi}{d\theta}, \quad (\text{B2})$$

and

$$\frac{dg_{\text{rad}}}{d\theta} = \left(\frac{4}{T} \frac{dT}{d\theta} + \frac{1}{v_\theta} \frac{dv_\theta}{d\theta} - \tan \theta \right) g_{\text{rad}}. \quad (\text{B3})$$

We can then rewrite equation (28a) as

$$\begin{aligned} \left[v_\theta^2 - \frac{4}{5} \frac{g_{\text{eff}}^2 - 2g_{\text{eff}}g_{\text{rad}} - 2g_{\text{rad}}v_\theta^2/R}{(g_{\text{eff}} - g_{\text{rad}})^2} \frac{kT}{\mu m_p} \right] \frac{dv_\theta}{d\theta} + \frac{8}{5} \frac{g_{\text{rad}}}{(g_{\text{eff}} - g_{\text{rad}})^2} \frac{v_\theta v_\phi}{R} \frac{kT}{\mu m_p} \frac{dv_\phi}{d\theta} + \left[\frac{4}{5} \frac{g_{\text{eff}}^2 + 3g_{\text{eff}}g_{\text{rad}}}{(g_{\text{eff}} - g_{\text{rad}})^2} v_\theta \right] \frac{d}{d\theta} \frac{kT}{\mu m_p} \\ = -F_\theta - F_{\text{cen}} - \frac{4}{5} \frac{g_{\text{eff}}^2 - 2g_{\text{eff}}g_{\text{rad}}}{(g_{\text{eff}} - g_{\text{rad}})^2} v_\theta \frac{kT}{\mu m_p} \tan \theta. \end{aligned} \quad (\text{B4})$$

From equation (28c), we must expand

$$\begin{aligned} \frac{d}{d\theta} \left[\frac{7g_{\text{eff}} + 3g_{\text{rad}}}{g_{\text{eff}} - g_{\text{rad}}} \frac{kT}{\mu m_p} \right] &= \frac{d}{d\theta} \left[\frac{10g_{\text{eff}} - 3(g_{\text{eff}} - g_{\text{rad}})}{g_{\text{eff}} - g_{\text{rad}}} \frac{kT}{\mu m_p} \right] = \frac{10g_{\text{eff}} - 3(g_{\text{eff}} - g_{\text{rad}})}{g_{\text{eff}} - g_{\text{rad}}} \frac{d}{d\theta} \frac{kT}{\mu m_p} + \frac{10}{g_{\text{eff}} - g_{\text{rad}}} \frac{kT}{\mu m_p} \frac{dg_{\text{eff}}}{d\theta} \\ &\quad - \frac{10g_{\text{eff}}}{(g_{\text{eff}} - g_{\text{rad}})^2} \frac{kT}{\mu m_p} \frac{d}{d\theta} (g_{\text{eff}} - g_{\text{rad}}). \end{aligned} \quad (\text{B5})$$

Using equations (B2) and (B3) we can then rewrite equation (28c) as

$$\left[v_\theta^2 + 4 \frac{g_{\text{eff}} g_{\text{rad}} + 2 g_{\text{rad}} v_\theta^2 / R}{(g_{\text{eff}} - g_{\text{rad}})^2} \frac{kT}{\mu m_p} \right] \frac{dv_\theta}{d\theta} + \frac{8 g_{\text{rad}}}{(g_{\text{eff}} - g_{\text{rad}})^2} \frac{v_\theta v_\phi}{R} \frac{kT}{\mu m_p} \frac{dv_\phi}{d\theta} + \left[\frac{27 g_{\text{eff}}^2 + 36 g_{\text{eff}} g_{\text{rad}} - 3 g_{\text{rad}}^2}{5 (g_{\text{eff}} - g_{\text{rad}})^2} v_\theta \right] \frac{d}{d\theta} \frac{kT}{\mu m_p} = F_\phi - F_{\text{cen}} - E_{\text{rad}} + \frac{4 g_{\text{eff}} g_{\text{rad}}}{(g_{\text{eff}} - g_{\text{rad}}) r} v_\theta \frac{kT}{\mu m_p} \tan \theta. \quad (\text{B6})$$

Equations (B4), (28b), and (B6) are of the form

$$A_1 \frac{dv_\theta}{d\theta} + A_2 \frac{dv_\phi}{d\theta} + A_3 \frac{d}{d\theta} \frac{kT}{\mu m_p} = C_1, \quad (\text{B7})$$

$$v_\theta v_\phi \frac{dv_\phi}{d\theta} = C_2, \quad (\text{B8})$$

$$B_1 \frac{dv_\theta}{d\theta} + B_2 \frac{dv_\phi}{d\theta} + B_3 \frac{d}{d\theta} \frac{kT}{\mu m_p} = C_3. \quad (\text{B9})$$

This can be inverted to find,

$$\frac{dv_\theta}{d\theta} = \frac{B_3 C_1 - A_3 C_3 + (A_3 B_2 - A_2 B_3) C_2 / (v_\theta v_\phi)}{A_1 B_3 - A_3 B_1}, \quad (\text{B10})$$

$$\frac{dv_\phi}{d\theta} = \frac{C_2}{v_\theta v_\phi}, \quad (\text{B11})$$

$$\frac{d}{d\theta} \frac{kT}{\mu m_p} = \frac{A_1 C_3 - B_1 C_1 + (A_2 B_1 - A_1 B_2) C_2 / (v_\theta v_\phi)}{A_1 B_3 - A_3 B_1}, \quad (\text{B12})$$

which can now be integrated numerically.

C. BOUNDARY CONDITION FOR LOW \dot{M}

Using the differential equations derived above, we can investigate the boundary condition $v_{\theta,0}$ in more detail. This reinforces that at low \dot{M} the solutions naturally attract toward the boundary condition of local viscous heating being balanced by local radiative cooling. In the limit of $\theta \approx 0$, $g_{\text{eff}} - g_{\text{rad}} \approx g_{\text{eff}} \approx GM/R^2 - v_\phi^2/R$, and $v_\phi \gg \sqrt{kT/(\mu m_p)}$, v_θ , the terms from above become

$$A_1 = v_\theta^2 - \frac{4}{5} \frac{kT}{\mu m_p} \approx -\frac{4}{5} \frac{kT}{\mu m_p}, \quad (\text{C1})$$

$$A_2 = 0, \quad (\text{C2})$$

$$A_3 = \frac{4}{5} v_\theta \quad (\text{C3})$$

$$B_1 = v_\theta^2 \quad (\text{C4})$$

$$B_2 = 0 \quad (\text{C5})$$

$$B_3 = \frac{14}{5} v_\theta \quad (\text{C6})$$

$$C_1 = -F_\theta \quad (\text{C7})$$

$$C_2 = -F_\phi \quad (\text{C8})$$

$$C_3 = F_\phi - E_{\text{rad}}. \quad (\text{C9})$$

In this limit, the derivative of v_θ , equation (B10), becomes,

$$\frac{dv_\theta}{d\theta} = \frac{-\frac{14}{5} F_\theta - \frac{4}{5} (F_\phi - E_{\text{rad}})}{-\frac{52}{25} kT/(\mu m_p) - \frac{4}{5} v_\theta^2} \approx \frac{35 F_\theta + 10 (F_\phi - E_{\text{rad}})}{26 kT/(\mu m_p)}. \quad (\text{C10})$$

Since $F_\theta \ll E_{\text{rad}}, F_\phi$, the second term in the numerator will dominate unless $E_{\text{rad}} = F_\phi$. If $F_\phi > E_{\text{rad}}$, then $dv_\theta/d\theta > 0$ and the solutions will be driven toward higher v_θ . From continuity, equation (24), this means that y must decrease. The radiative cooling is $E_{\text{rad}} \propto g_{\text{rad}} v_\theta \propto y^{-2}$ so that it will increase, pushing the solutions toward local energy balance. If $E_{\text{rad}} > F_\phi$, then $dv_\theta/d\theta < 0$ and once again local energy balance is reached for similar reasons. The only time $dv_\theta/d\theta$ will vary slowly is when $E_{\text{rad}} = F_\phi$ and we see in this case $dv_\theta/d\theta \approx 35 F_\theta / [26 kT/(\mu m_p)]$, which is positive. This is consistent with initial slope of v_θ in Figures (2) and (6). More detailed analysis, including the effects of g_{rad} , is needed to correctly predict the values of the slopes seen.

REFERENCES

- Frank, J., King, A. R. & Raine, D. J. 2002, *Accretion Power in Astrophysics*, (3d ed.; Cambridge: Cambridge Univ. Press)
- Heise, J., van Teeseling, A. & Kahabka, P. 1994, *A&A*, 288, 45
- Huang, M., Sion, E. M., Hubeny, I., Cheng, F. H. & Szkody, P. 1996a, *ApJ*, 458, 355
- Huang, M., Sion, E. M., Hubeny, I., Cheng, F. H. & Szkody, P. 1996b, *AJ*, 111, 2386
- Inogamov, N. A. & Sunyaev, R. A. 1999, *Astron. Lett.*, 25, 269 (IS99)
- Kippenhahn, R. & Thomas, H.-C. 1978, *A&A*, 63, 265
- Kley, W. 1989a, *A&A*, 208, 98
- Kley, W. 1989b, *A&A*, 222, 141
- Kley, W. & Hensler, G. 1987, *A&A*, 172, 124
- Landau, L. D. & Lifshitz, E. M. 1959, *Fluid Mechanics* (London: Pergamon)
- Long, K. S., Mauche, C. W., Raymond, J. C., Szkody, P. & Mattei, J. A., *ApJ*, 469, 841
- Mauche, C. W. 1996, in *Cataclysmic Variables and Related Objects*, ed. A. Evans & J. H. Wood (Dordrecht: Kluwer), 243
- Mauche, C. W., Mattei, J. A. & Bateson, F. M. 2001, *ASP Conf. Ser.* 229, in *Evolution of Binary and Multiple Stars*, ed. P. Podsiadlowski et al. (San Francisco: ASP), 367
- Mauche, C. W. & Raymond, J. C. 2000, *ApJ*, 541, 924
- Mauche, C. W., Raymond, J. C. & Mattei, J. A. 1995, *ApJ*, 446, 842
- Meyer, F. & Meyer-Hofmeister, E. 1982, *A&A*, 106, 34
- Mürset, U., Nussbaumer, H., Schmid, H. M. & Vogel, M. 1991, *A&A*, 248, 458
- Narayan, R. & Popham, R. 1993, *Nature*, 362, 820
- Popham, R. & Narayan, R. 1995, *ApJ*, 442, 337
- Pringle, J. E. 1977, *MNRAS*, 178, 195
- Pringle, J. E. 1981, *ARA&R*, 19, 137
- Pringle, J. E. & Savonije, G. J. 1979, *MNRAS*, 187, 777
- Rosner, R., Alexakis, A., Young, W.-N., Truran, J. W. & Hillebrandt W. 2001, *ApJ*, 562, 177
- Shakura, N. I. & Sunyaev, R. A. 1973, *A&A*, 24, 337
- Sion, E. M. 1999, *PASP*, 111, 532
- Sion, E. M., Cheng, F. H., Huang, M., Hubeny, I. & Szkody, P. 1996, *ApJ*, 471, L41
- Sokoloski, J. L., Bildsten, L. & Ho, W. C. G. 2001, *MNRAS*, 326, 553
- Spitzer, L. 1965, *Physics of Fully Ionized Gases* (New York: Interscience)
- Townsley, D. M. & Bildsten, L. 2003, *ApJ*, 596, 227
- Tylenda, R. 1977, *Acta Astron.*, 27, 235
- Tylenda, R. 1981, *Acta Astron.*, 31, 267
- van den Heuvel, E. P. J., Bhattacharya, D., Nomoto, K. & Rappaport, S. A. 1992, *A&A*, 262, 97
- Warner, B. 1995, *Cataclysmic Variable Stars* (Cambridge: Cambridge Univ. Press)
- Wheatley, P. J., Mauche, C. W. & Mattei, J. A. 2003, *MNRAS*, 345, 49 (WMM03)